Spin-flip processes and nondipole effects in above-threshold ionization of hydrogen in ultrastrong laser fields

I. A. Ivanov*

Center for Relativistic Laser Science, Institute for Basic Science, 123 Cheomdangwagiro, Buk-gu, Gwangju 61005, Korea and Research School of Physics and Engineering, The Australian National University, Canberra, Australian Capital Territory 0200, Australia

(Received 25 May 2017; revised manuscript received 19 June 2017; published 20 July 2017)

We consider above-threshold ionization of hydrogen atoms in ultrastrong laser fields. We use a time-dependent Dirac equation as a calculational tool. This framework allows one to include relativistic effects such as nondipole effects, effects of the relativistic kinematics, and electron spin effects. Inclusion of the spin effects allows one to consider the spin-flip process accompanying above-threshold ionization. We present and discuss electron momenta distributions for ionization processes with and without spin flips. Electron momenta distributions for the ionization process without a spin flip show a gradual increase of the role of the nondipole effects with increasing electric field. Electron spectra for the spin-flip ionization exhibit cusplike singularities, and the absence of features (such as the presence of dips) in the case of the ionization without a spin flip. We explain these features by invoking perturbation theory arguments.

DOI: 10.1103/PhysRevA.96.013419

I. INTRODUCTION

It has been realized since the pioneer paper by Reiss [1] that relativistic effects may play a significant role in the process of atomic or molecular photoionization. Even for infrared (IR) laser fields of moderate intensity of the order of 1×10^{13} W/cm^2, in the so-called tunneling regime of ionization, the relativistic nondipole effects are visible in the experimentally observed photoelectron spectra [2]. Each IR photon carries small momentum, but a large number of the photons participating in the process of the tunneling ionization [3] deliver appreciable momentum to the ionized electron. Nondipole effects accompanying multiphoton processes in this regime of ionization have been studied extensively experimentally [2,4] and theoretically [5–10].

Another group of effects, which relativity introduces into the theory of strong field ionization, includes the effects related to the electron spin. It was shown [11] that for field intensities of the order of 1×10^{14} W/cm^2 strong spin asymmetry can be observed in the above-threshold ionization (ATI) process driven by counter-rotating two-color circularly polarized fields, which introduces the field of spin-related effects into attoscience. The qualitative theory of tunneling ionization in very strong fields, describing the ATI process and taking into account the spin effects, in particular the spin-flip processes, was developed in [10].

Development of free-electron lasers (FELs) [12–14] opened up the possibility of experimental study of the relativistic effects for multiphoton processes in the domain of high photon energies, where the nondipole effects due to finite photon momentum can be expected to be particularly important. That this is indeed the case was shown in [15], where a nonperturbative study of ATI in superintense and ultrashort wavelength was reported. It was found that inclusion of the nondipole effects may modify ATI spectra appreciably. The $\mathcal{P}$-space method used in this work treated nonperturbatively the nondipole effects but did not include effects due to electron spin.

In the present work we report a study of the ATI of a hydrogen atom subjected to superintense extreme ultraviolet radiation. We base our study on the recently developed procedure [16] that allows one to solve the three-dimensional (3D) time-dependent Dirac equation (TDDE). This framework incorporates naturally electron spin effects, which allows one to consider ATI processes with and without electron spin flip. Below we present results for both (with and without spin flip) ATI processes.

The paper is organized as follows. In Sec. II we describe the numerical technique we use to perform the TDDE calculation. Our results and conclusions drawn are presented in Secs. III and IV, respectively. Atomic units with $\hbar = 1$, $e = 1$, $m = 1$, and $c \approx 137.036$ (here e and m are charge and mass of the electron, and c is the speed of light) are used throughout the paper.

II. THEORY

A. Solution of the time-dependent Dirac equation

We solve the TDDE for the hydrogen atom in the field of a laser pulse:

$$i\frac{\partial \Psi(\boldsymbol{r},t)}{\partial t} = \hat{H}\Psi(\boldsymbol{r},t), \tag{1}$$

where $\Psi(\boldsymbol{r},t)$ is a four-component wave function (bispinor), and $\hat{H}$ is the Hamiltonian operator,

$$\hat{H} = \hat{H}_{\rm atom} + \hat{H}_{\rm int}, \tag{2}$$

with

$$\hat{H}_{\rm atom} = c\boldsymbol{\alpha}\cdot\hat{\boldsymbol{p}} + c^2(\beta - I) - \frac{I}{r} \tag{3}$$

and

$$\hat{H}_{\rm int} = c\boldsymbol{\alpha}\cdot\boldsymbol{A}. \tag{4}$$

*Igor.Ivanov@anu.edu.au

In Eq. (3),

$$\boldsymbol{\alpha} = \begin{pmatrix} \mathbf{0} & \boldsymbol{\sigma} \\ \boldsymbol{\sigma} & \mathbf{0} \end{pmatrix}, \quad \beta = \begin{pmatrix} \boldsymbol{I} & \mathbf{0} \\ \mathbf{0} & -\boldsymbol{I} \end{pmatrix}, \quad I = \begin{pmatrix} \boldsymbol{I} & \mathbf{0} \\ \mathbf{0} & \boldsymbol{I} \end{pmatrix},$$

$\boldsymbol{\sigma}$ are Pauli matrices, $\mathbf{0}$ and $\boldsymbol{I}$ are 2×2 null and identity matrices, and c is the speed of light. We subtracted from the field-free atomic Hamiltonian (3) the constant term Ic^2 corresponding to rest mass energy of the electron.

Interaction of the atom and the external electromagnetic field is described using the Coulomb gauge. We choose a particular geometry in which the laser pulse is linearly polarized along the z direction and propagates in the x direction, so the vector potential in Eq. (4) is of the form

$$\boldsymbol{A}(\boldsymbol{r},t) = \hat{\boldsymbol{z}} h(\zeta), \tag{5}$$

where $\hat{\boldsymbol{z}}$ is a unit vector along the z axis, $\zeta = t - \frac{x}{c}$, and $h(\zeta)$ has a compact support [i.e., it is zero outside an interval $(0,T)$] for a pulse of finite temporal duration and spatial extension. We use a particular form of this function corresponding to the sine-squared envelope of the vector potential:

$$h(\zeta) = -\frac{F}{\omega} \sin^2\left(\frac{\Omega\zeta}{2}\right) \sin(\omega\zeta) \tag{6}$$

for $\zeta \in (0,T)$ and zero otherwise. The parameter T denotes the total pulse duration (as measured at any given spatial point), $\Omega = 2\pi/T$, and F is the strength of the electric field of the pulse. We employ here the definition of the vector potential commonly used in atomic physics so that electric and magnetic field vectors are related to the vector potential as $\boldsymbol{F}(t - x/c) = -\hat{\boldsymbol{z}} \frac{\partial A(t-x/c)}{\partial t}$ and $\boldsymbol{H}(t - x/c) = -c\hat{\boldsymbol{y}} \frac{\partial A(t-x/c)}{\partial x}$, where $\hat{\boldsymbol{z}}$ and $\hat{\boldsymbol{y}}$ are unit vectors along the z and y directions, respectively.

Values for other parameters defining the laser pulse were as follows. The carrier frequency was $\omega = 5.0042$ a.u., corresponding to a wavelength of 9.11 nm. Calculations were performed for the following values of the parameter T: $T = 3T_1$, $T = 5T_1$, and $T = 10T_1$, where $T_1 = 2\pi/\omega$ is an optical cycle (o.c.) corresponding to the carrier frequency ω. The pulse shape and the carrier frequency we employ coincide with those used in [15], thereby enabling comparison of the results obtained by different methods.

The procedure used to solve the TDDE was described in [16]; we only briefly mention the most essential details. The solution is represented as a series in basis bispinors:

$$\Psi(\boldsymbol{r},t) = \sum_{\substack{j \\ l=j\pm 1/2}}^{J_{\max}} \sum_{M=-j}^{j} \Psi_{jlM}(\boldsymbol{r},t), \tag{7}$$

where each basis bispinor is

$$\Psi_{jlM}(\boldsymbol{r},t) = \begin{pmatrix} g_{jlM}(r,t)\Omega_{jlM}(\boldsymbol{n}) \\ f_{jlM}(r,t)\Omega_{jl'M}(\boldsymbol{n}) \end{pmatrix}, \tag{8}$$

and two-component spherical spinors are defined as $\Omega_{jlM}(\boldsymbol{n}) = \begin{pmatrix} C^{jM}_{l\,M-\frac{1}{2}\,\frac{1}{2}\,\frac{1}{2}} Y_{l,M-\frac{1}{2}}(\boldsymbol{n}) \\ C^{jM}_{l\,M+\frac{1}{2}\,\frac{1}{2}-\frac{1}{2}} Y_{l,M+\frac{1}{2}}(\boldsymbol{n}) \end{pmatrix}$ [here $C^{jM}_{lm\frac{1}{2}\mu}$ are the Clebsch-Gordan coefficients, $Y_{lm}(\boldsymbol{n})$ are the spherical harmonics, and $\boldsymbol{n} = \boldsymbol{r}/r$]. Parameters l and l' in Eq. (7) must satisfy the relation $l + l' = 2j$.

To take into account nondipole effects due to the spatial dependence of the laser fields, vector potential (5) is expanded in a series of spherical harmonics at every step of the integration procedure.

After some cumbersome, albeit straightforward, manipulations using well-known properties of spherical spinors [17,18], this strategy results in a set of coupled differential equations for the radial functions $g_{jlM}(r,t)$ and $f_{jlM}(r,t)$ in Eq. (8), describing propagation of the TDDE in time. This system is solved using a relativistic generalization of the well-known matrix iteration method (MIM) [19], which we described in detail in [16].

B. Distribution of photoelectrons

Angle-integrated photoelectron spectra $dP(E)/dE$ are obtained by projecting the solution of the TDDE after the end of the pulse on the set of the continuum states $\Psi_{jlM}(\boldsymbol{r})$ of the hydrogen atom [17] and summing over all possible jlM. We also present below the spin-resolved differential distributions $P(\mu,\boldsymbol{p}) = |a(\mu,\boldsymbol{p})|^2$ which are calculated by computing ionization amplitudes $a(\mu,\boldsymbol{p})$, where μ is polarization (i.e., spin direction in the electron's rest frame) and $\boldsymbol{p}$ is asymptotic electron momentum. The amplitudes are obtained by projecting the solution of the TDDE after the end of the pulse on the set of the ingoing relativistic scattering states $\Psi^-_{\mu,\boldsymbol{p}}(\boldsymbol{r})$ of the hydrogen atom [17]:

$$\Psi^-_{\mu,\boldsymbol{p}}(\boldsymbol{r}) = \sum_{jlM} i^l e^{-i\delta_{jl}(p)} \langle \Omega_{jlM}(\hat{\boldsymbol{p}}) | v_\mu \rangle \Psi_{pjlM}(\boldsymbol{r}), \tag{9}$$

where $\Psi_{pjlM}(\boldsymbol{r})$ are continuous spectrum wave functions of the Dirac Hamiltonian normalized to $\delta(p - p')$, $\delta_{jl}(p)$ is the relativistic Coulomb phase shift, $\Omega_{jlM}(\hat{\boldsymbol{p}})$ is a two-component spherical spinor, and v_μ is a two-component spinor describing the polarization state.

To gauge the role of nondipole effects, we are also interested below in the distribution of the electron momentum component along the laser beam propagation direction. For the geometry we employ, a laser beam propagating along the x axis, this distribution can be computed as

$$W(\mu,p_x) = \int P(\mu,\boldsymbol{p})\, dp_y\, dp_z, \tag{10}$$

with differential probability $P(\mu,\boldsymbol{p})$ defined above.

C. Details of the numerical procedure

Spatial variables in the coupled differential equations for the radial functions $g_{jlM}(r,t)$ and $f_{jlM}(r,t)$ were discretized on a grid with step size $\delta r = 0.02$ a.u.; the radial variable was restricted to an interval $(0,R_{\max})$, with $R_{\max} = 600$ a.u. The initial ground state of the hydrogen atom with total angular momentum $j = 1/2$, and its projection on the z axis $M = 1/2$, was prepared by solving the eigenvalue problem for the discretized Hamiltonian, resulting in a ground-state energy of -0.500006657 a.u., which is to be compared with the value -0.5000066566 a.u. given by the Dirac formula. [To facilitate comparison with the nonrelativistic calculations, we subtracted the rest mass energy term mc^2 in Hamiltonian (3)].

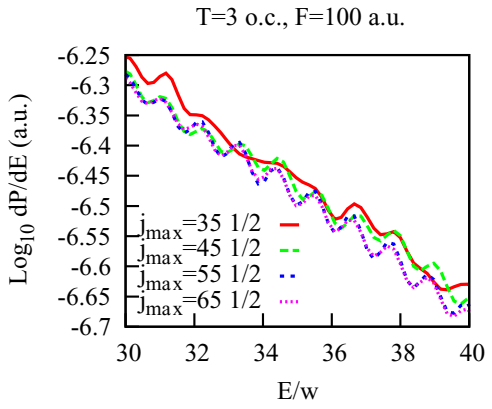

FIG. 1. Angular integrated photoelectron spectra for different values of the parameter $J_{\max}$ in Eq. (7) for the pulse duration $T = 3$ o.c. and field strength $F = 100$ a.u. Angular integrated differential probability dP/dE is plotted against the ratio E/ω of the electron energy and the pulse frequency.

In this work we consider very strong electromagnetic fields (electric field strength of up to 100 a.u., i.e., a field intensity of 3.51×10^{20} W/cm^2). Proper care, therefore, should be exercised to ensure that results of the calculations are indeed accurate. One of the key parameters governing the accuracy of the calculational strategy we described above is the step size Δt used for the propagation of the TDDE in time. This parameter was controlled by performing a sequence of calculations with ever-decreasing time steps. The convergence on the level of a percent, which we deemed acceptable, was found for $\Delta t = 0.05$ a.u. for the field strength $F = 10$ a.u., $\Delta t = 0.01$ a.u. for $F = 30$ a.u., $\Delta t = 0.0025$ a.u. for $F = 50$ a.u., and $\Delta t = 0.0005$ a.u. for $F = 100$ a.u. Another important parameter which may have a crucial impact on the overall accuracy of the calculation is the parameter $J_{\max}$, the maximum value of the total momentum j in Eq. (7). After the necessary convergence tests we adopted the following values for $J_{\max}$: $J_{\max} = 30\frac{1}{2}$ for $F = 10$ a.u., $J_{\max} = 40\frac{1}{2}$ for $F = 10$ a.u., $J_{\max} = 45\frac{1}{2}$ for $F = 50$ a.u., and $J_{\max} = 65\frac{1}{2}$ for $F = 100$ a.u.

Figure 1 shows that even for the very high field strength of $F = 100$ a.u. we were able to obtain well-converged results for the total angle-integrated ionization probability summed over all electron spin projections in the final state. Below we also present results for the spin-resolved ionization probabilities, corresponding to the ionization with and without spin flip. For the field parameters we consider that the spin-flip ionization probability is much smaller than the ionization probability without spin flip. Figure 1, therefore, which presents results which are dominated by the much larger probability of ionization without spin flip, cannot tell us much about the accuracy of the results for the spin-flip ionization probability we obtain. A special investigation is needed in this case. We present results of the corresponding accuracy checks below when discussing the spin-flip ionization process.

III. RESULTS AND DISCUSSION

In Fig. 2 we show results for the angular integrated ATI spectra obtained for various pulse durations and field strengths, following the calculational procedure described above. We show results of the fully relativistic calculation, using the solution of the TDDE and nonrelativistic calculation entirely neglecting nondipole effects and relativistic kinematics. The latter results, denoted as the time-dependent Schrödinger equation (TDSE) in Fig. 2, have been obtained using the nonrelativistic version of the relativistic procedure we described above, by replacing Hamiltonian operators (3) and (4) with their nonrelativistic counterparts and representing the wave function as a series in spherical harmonics as in Eq. (7), with the difference that the nonrelativistic wave function has but one component (we neglect, of course, all spin effects in the TDSE calculation). The parameters responsible for the overall accuracy of the calculation were chosen as in the relativistic case by performing the necessary convergence tests. We do not dwell upon this issue for the nonrelativistic calculation; it was described in detail elsewhere [20,21].

We present in Fig. 2 results for the field strengths of $F = 30$, $F = 50$, and $F = 100$ a.u., and pulse durations of $T = 3$, 5, and 10 o.c. The region of the field strengths $F \leqslant 50$ a.u. was considered in [15] [with pulse parameters identical to those used in Eq. (6)]. For the sake of comparison we show in Fig. 2 the spectra obtained in [15] for the following sets of field parameters: $F = 30$ a.u., $T = 3$ o.c.; $F = 30$ a.u., $T = 10$ o.c.; and $F = 50$ a.u., $T = 10$ o.c. We obtained these data by electronically scanning the figures that showed corresponding spectra in [15]. We do not perform, therefore, a detailed comparison of the data, which would be meaningless using the scanned data. We can, however, draw general conclusions regarding the overall agreement of the results. One can see that the spectral intensities given by the present TDSE and TDDE calculations generally agree very well with the results of the calculation relying on the $\mathcal{P}$- space approach advocated in [15], as long as we consider the region of relatively low energies not exceeding approximately $20\omega \approx 100$ a.u. One can observe from Fig. 2 that electron energy of approximately 100 a.u. is at the same time the energy at which our relativistic TDDE results begin to deviate appreciably from the results of the nonrelativistic TDSE calculation. For the electron energy of approximately 100 a.u. the ratio of the electron velocity and the speed of light is $v/c \approx 0.1$. For such relatively small velocities is it still meaningful to classify contributions of the various relativistic effects according to the leading order of the expansion in the powers of $\lambda = 1/c$ in which these effects manifest themselves if relativistic effects are treated perturbatively. The contribution of the leading-order nondipole effects is proportional to λ. We give an explicit expression for the Hamiltonian including relativistic effects to this order (we use it below). This expression can be obtained by expanding the vector potential $\boldsymbol{A}(t - x/c)$ in powers of x/c and keeping the first two terms of this expansion, resulting in the Hamiltonian $\hat{H}^1$ describing effects of up to first order in the parameter $\lambda = 1/c$ [7]:

$$\hat{H}^1 = \frac{\hat{\boldsymbol{p}}^2}{2} - \frac{1}{r} + \hat{p}_z A(t) + \frac{\hat{p}_z x E(t)}{c} + \frac{A(t)E(t)x}{c} - \frac{\sigma_y H(t)}{2c}, \tag{11}$$

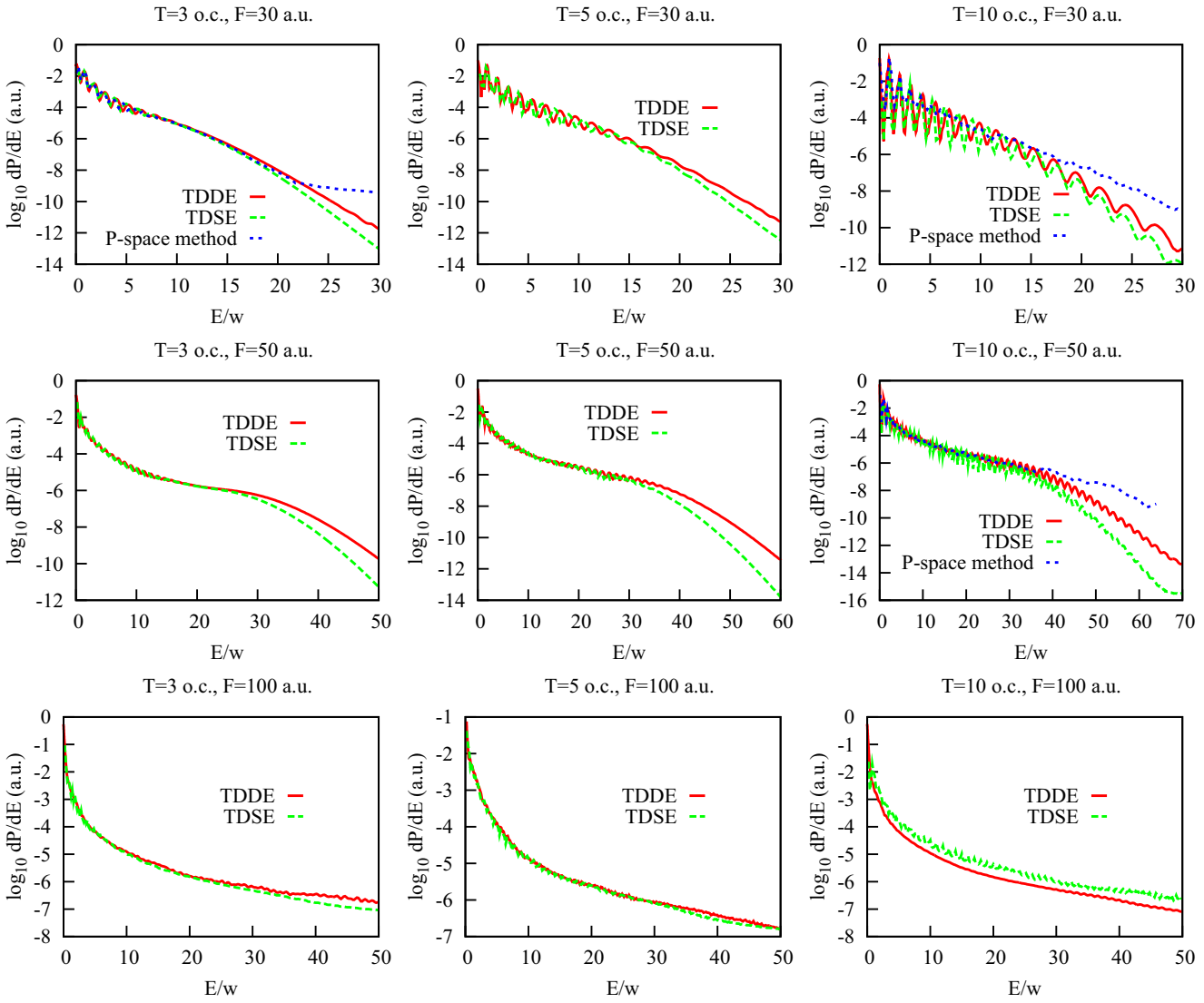

FIG. 2. Angular integrated photoelectron spectra for different values of the total pulse duration and field strength. Differential probabilities dP/dE are plotted against the ratio E/ω of the electron energy and the pulse frequency. $\mathcal{P}$-space results of the work [15] are shown for comparison.

where the last term describes the interaction of the magnetic field of the pulse and electron's spin. The relativistic effects due to the relativistic kinematics and effects due to the coupling of the spin and spatial variables are of the order of λ^2 [22]. The fact that the TDSE and the TDDE results in Fig. 2 begin to deviate at the electron energies of approximately 100 a.u. is, therefore, easy to understand; the magnitude of the leading-order correction describing the nondipole effects is of the order of $v/c \approx 0.1$ for this energy. Less clear is the origin of the discrepancy of the TDDE results and the results of calculations [15] using the $\mathcal{P}$-space method. As we mentioned above, we have carefully examined convergence of our calculations with respect to the essential parameters governing the overall accuracy, such as the parameter $J_{\max}$ defining angular momentum composition of the wave function, integration time step, or coordinate grid size and step. Convergence with respect to the parameter $J_{\max}$ has been illustrated above in Fig. 1. We note that the values for the parameter $J_{\max}$ we had to choose in the present calculation to achieve convergence are somewhat higher than the values of the analogous parameter L_{M} in the calculations reported in [15]. It was found in [15] that L_{M} of the order of 10 allowed one to achieve convergence of the partial wave expansion used in this work for an electric field strength of 50 a.u. This difference of the number of partial waves taken into account in the calculations might be responsible for the observed difference of the results. One should take into account, however, that the partial wave expansion used in [15] represented the wave function in the momentum $\mathcal{P}$ space, while our expansion (7) represents the wave function in the coordinate $\mathcal{R}$ space. Convergence properties of the partial wave expansions in the two spaces may, of course, be quite different.

TDSE spectra for the pulse duration of 10 o.c. and field strength of 50 and 100 a.u. in Fig. 2 look less smooth than the TDDE results. Figure 3 zooms on the spectral intervals where this behavior of the TDSE results is most noticeable.

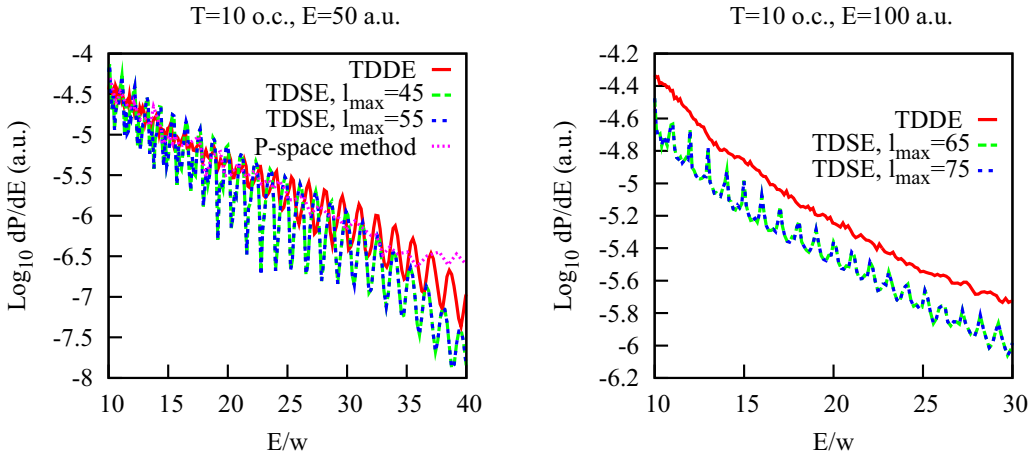

FIG. 3. Magnified view of the angular integrated photoelectron spectra for different values of the total field strength and pulse duration of 10 o.c. Distributions dP/dE are plotted against the ratio E/ω of the electron energy and the pulse frequency. $\mathcal{P}$-space results of [15] are shown for comparison.

One can see that, under magnification, the "noise" in the TDSE results resolves into well-defined maxima of the ATI spectra. To illustrate that this behavior is not related to a lack of convergence of the TDSE results, we present in Fig. 3 these results for two values of the parameter $l_{\max}$ [the nonrelativistic analog of the parameter $J_{\max}$ in Eq. (7), which defines the number of the partial waves used in the TDSE calculation]. Results of the two nonrelativistic calculations agree very well. The smoother dependence of the nondipole dP/dE on the photon energy, compared to the nonrelativistic results, visible for some spectra in Fig. 2, is, therefore, a consequence of the fact that ATI peaks are less well resolved in the nondipole case. This fact agrees with the observation made in [15].

The role of the nondipole effects is illustrated in Figs. 4, 5, and 6, where we present two-dimensional distributions $W(\mu, p_x, p_z) = P(\mu, p_x, 0, p_z)$, describing distributions of momenta of the photoelectrons in the (x,z) plane for different field strengths and pulse durations. For the ionization channel

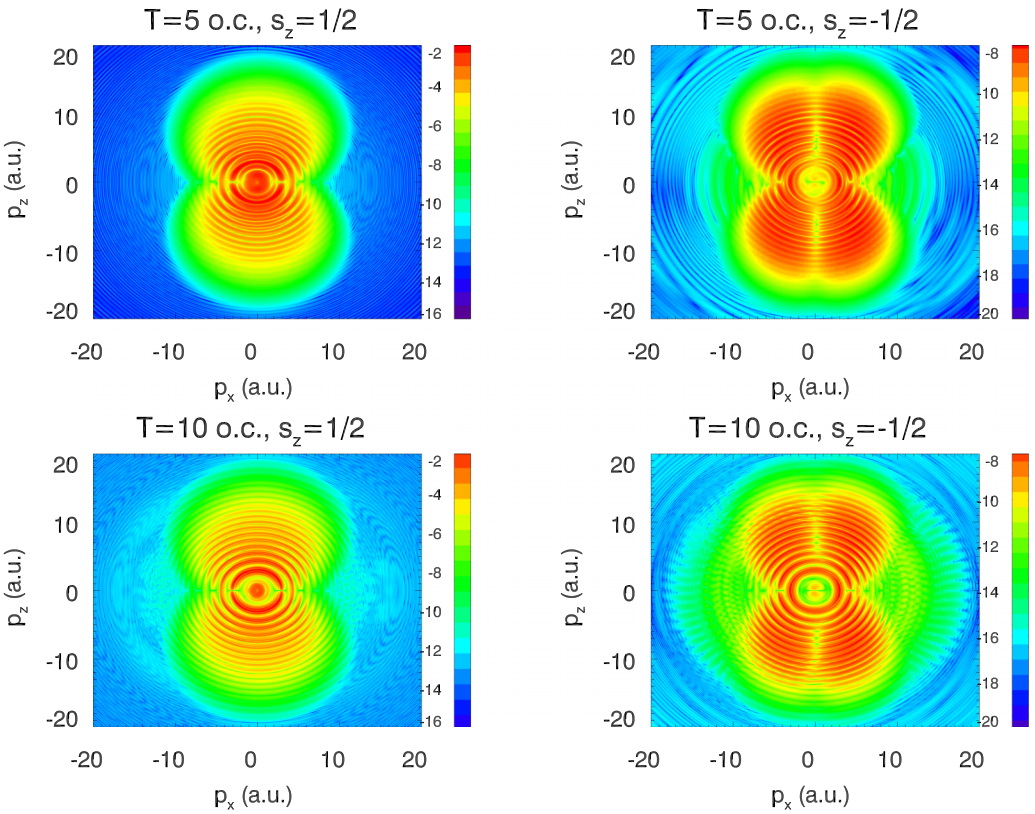

FIG. 4. Ionization probability distribution in the (p_x, p_z) plane for the pulse electric field strength $F = 30$ a.u. into the final states with $s_z = 1/2$ and $s_z = -1/2$. Logarithmic scale is used.

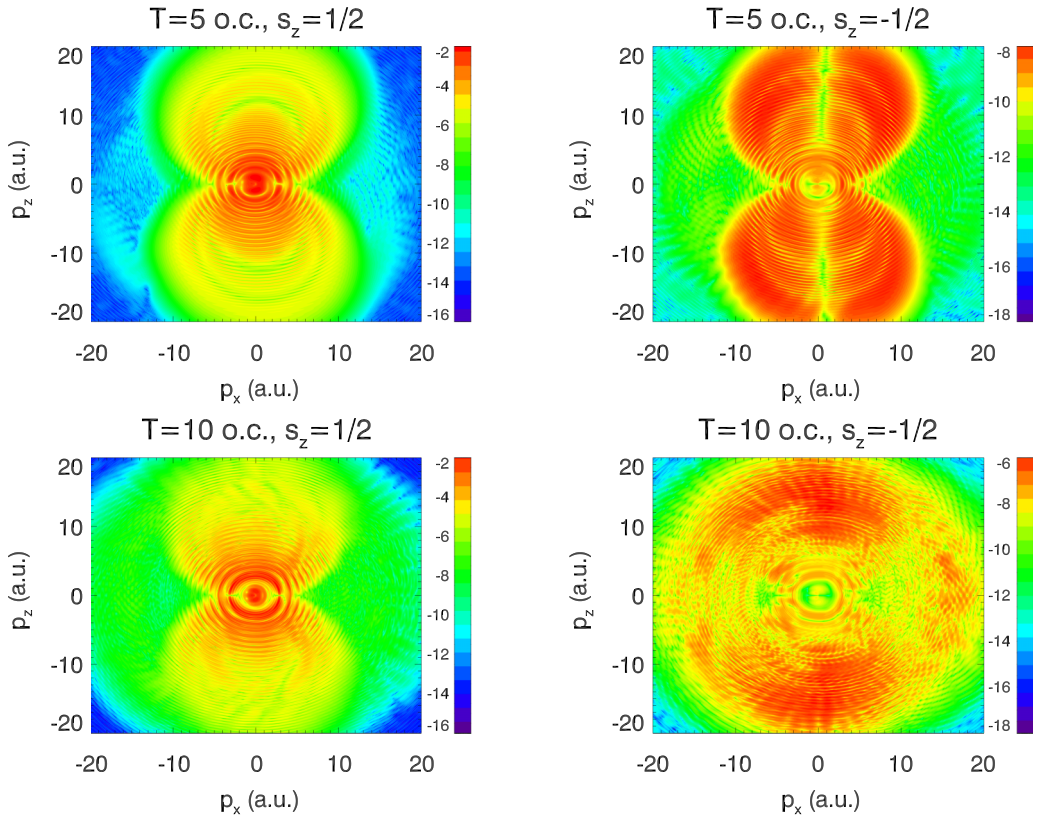

FIG. 5. Ionization probability distribution in the (p_x, p_z) plane for the pulse electric field strength $F = 50$ a.u. into the final states with $s_z = 1/2$ and $s_z = -1/2$. Logarithmic scale is used.

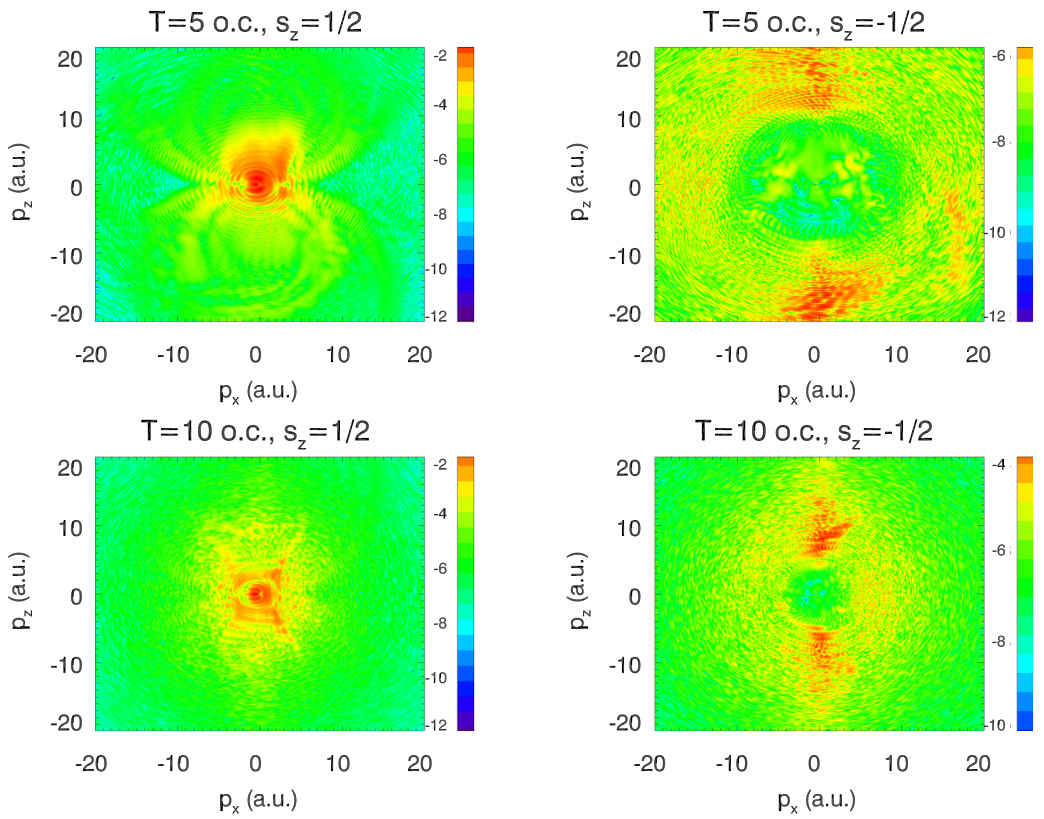

FIG. 6. Ionization probability distribution in the (p_x, p_z) plane for the pulse electric field strength $F = 100$ a.u. into the final states with $s_z = 1/2$ and $s_z = -1/2$. Logarithmic scale is used.

corresponding to a spin-flip process ($\mu = -1/2$), the distributions $W(\mu, p_x, p_z)$ exhibit a dip along $p_x = 0$.

The presence of this structure for not very high field strengths can be understood using the following simple arguments based on the perturbation theory considering relativistic effects as a perturbation. We should bear in mind, of course, that for the field strengths we consider, an approach based on the perturbation theory can have, at best, a qualitative explanatory power. Spin-flip processes are only possible if coupling of the spin and spatial variables is introduced in the Hamiltonian. Hamiltonian $\hat{H}^1$ which we introduced in Eq. (11) includes the relativistic effects up to the first order in powers of the parameter $\lambda = 1/c$. Effects of the order of λ^2 are obtained if we include the relativistic kinematic effects and, more importantly for the purpose of the discussion of the spin-flip processes, if we take into account the dependence of the magnetic field in the last term in Eq. (11) on the spatial coordinates. With the accuracy of up to second order in λ this leads to the terms in the Hamiltonian:

$$\frac{\sigma_y H(t - x/c)}{2c} \approx \frac{\sigma_y H(t)}{2c} - \sigma_y \frac{x}{2c^2} \frac{\partial H(t)}{\partial t}. \tag{12}$$

The last term on the right-hand side of Eq. (12) introduces the coupling of the spin and spatial variables. In the Hamiltonian $\hat{H}^2$, including relativistic effects of up to second order in the parameter $\lambda = 1/c$, we have then two different operators describing the electron-field interaction:

$$\begin{aligned} \hat{V}_x &= -\sigma_y \frac{x}{2c^2} \frac{\partial H(t)}{\partial t}, \\ \hat{V}_z &= \hat{p}_z A(t) + \frac{\hat{p}_z x E(t)}{c} + \frac{A(t) E(t) x}{c}, \end{aligned} \tag{13}$$

where we used Eq. (11) to obtain the expression for $\hat{V}_z$. Adopting the picture of photons, we may say that operator $\hat{V}_z$ is responsible for the absorption of a photon without a spin flip (it is diagonal with respect to the spin variables), while $\hat{V}_x$ is responsible for the absorption of a photon accompanied by a spin flip (this operator couples spin-up and spin-down states). The perturbation theory expression for the amplitude a_f for the ionization into a final state $|f\rangle = |\mu, \boldsymbol{p}\rangle$ corresponding to an absorption of N photons can be written as

$$a_f \propto \sum_{\nu_1, \nu_2, \ldots, \nu_{N-1}} \hat{V}_{f\nu_1} \hat{V}_{\nu_1 \nu 2} \cdots \hat{V}_{\nu_{N-1} i} \Phi(\nu, \omega), \tag{14}$$

where $|i\rangle$ is an initial state, ν_i is a complete set of the intermediate states, and $\Phi(\nu, \omega)$ are some coefficients, depending on the energies of the states $|i\rangle$ and ν_i and photon frequency ω. We can use now the fact that the photon frequency we consider is relatively large, so the factors $\Phi(\nu, \omega)$ can be considered functions of the photon frequency only (this is the well-known closure approximation). We may perform then the summations over the intermediate states ν_i using completeness relations for the sets of the states $|\nu_i\rangle$. Under the closure approximation the sum in Eq. (14) reduces to

$$a_f \propto \langle f | \hat{V}_1 \hat{V}_2 \cdots \hat{V}_N | i \rangle, \tag{15}$$

where each operator $\hat{V}_i$ is either operator $\hat{V}_x$ or operator $\hat{V}_z$. For the final state $|f\rangle = |\mu = -1/2, \boldsymbol{p}\rangle$, corresponding to a spin-flip process, considered in the lowest nonvanishing order of the perturbation theory, we must clearly have in Eq. (15) $N - 1$ operators $\hat{V}_z$ and one operator $\hat{V}_x$. If we are interested in the lowest order in $1/c$ we may, moreover, use expression $\hat{V}_z = \hat{p}_z A(t)$ for the V_z, neglecting in Eq. (13) terms of the order of $1/c$. Equation (15) can then be written as

$$a_{\mu=-1/2, \boldsymbol{p}} \propto \langle f | \hat{p}_z^{N-1} \hat{x} | i \rangle, \tag{16}$$

where we used the fact that, under the assumptions we have made, all the operators $\hat{V}_i$ in Eq. (15) commute. Dependence of the amplitude (15) on the direction of the vector $\boldsymbol{p}$ can easily be obtained using standard techniques of calculations of the matrix elements of tensor operators [22]. It is more straightforward to do that, however, assuming that we use a plane wave for the final state $|f\rangle$ (which is a good approximation for the high energies we consider). We obtain then, substituting in Eq. (16) $x e^{i \boldsymbol{p} \cdot \boldsymbol{r}} = -i \frac{\partial}{\partial p_x} e^{i \boldsymbol{p} \cdot \boldsymbol{r}}$,

$$a_{\mu=-1/2, \boldsymbol{p}} \propto p_z^{N-1} \frac{\partial \tilde{\phi}(\boldsymbol{p})}{\partial p_x} \propto p_z^{N-1} p_x, \tag{17}$$

where we introduced Fourier transform $\phi(\boldsymbol{p})$ of the ground-state wave function of the hydrogen atom and used the fact that $\phi(\boldsymbol{p})$ in this case is a function of $\boldsymbol{p}^2$, so that p_x differentiation in Eq. (17) introduces a factor p_x. Under the closure approximation the perturbative amplitude for the spin-flip process, therefore, has a node along the line $p_x = 0$, which explains the origin of the dip along the line $p_x = 0$ exhibited by the spin-flip distributions. Expression (17) also predicts low ionization probability density for small p_z in agreement with the results shown in Figs. 4 and 5.

An analogous derivation would give the following for the amplitude of the ionization due to absorption of N photons for the process without spin flip:

$$a_{\mu=1/2, \boldsymbol{p}} \propto p_z^{N-1} \frac{\partial \tilde{\phi}(\boldsymbol{p})}{\partial p_x} \propto p_z^{N}, \tag{18}$$

which does not account for the presence of the considerable amount of ionized electrons with small p_z which can be observed in Figs. 4–6. We should note, however, that the processes without spin flip can in no way be considered a perturbation for the field strengths we consider. It is the presence of the small factor c^{-2} in expression (13) for $\hat{V}_x$ which makes the perturbation theory approach not hopelessly inadequate in the case of ionization accompanied by a spin-flip process.

A feature which becomes clearly visible in the distributions present in Figs. 4–6 for the ionization without a spin flip is asymmetry with respect to the reflection operation $p_x \to -p_x$, growing with the increasing field strength, which is a manifestation of the nondipole effects. The asymmetry with respect to the operation $p_z \to -p_z$, which is also visible in the figures, arises because we use relatively short laser pulses and is of no interest to us. For the ionization accompanied by a spin flip, and for lower field strengths, the distributions $W(\mu = -1/2, p_x, p_z)$ are also symmetric with respect to the reflection $p_x \to -p_x$, in agreement with the perturbative expression for the ionization amplitude (17) we derived above. The departure from the $p_x \to -p_x$ symmetry for higher field strengths is rather a manifestation of the breakdown of the perturbation theory in this case. The $p_x \to -p_x$ symmetry following from the perturbative expression (17) is still present for a shorter

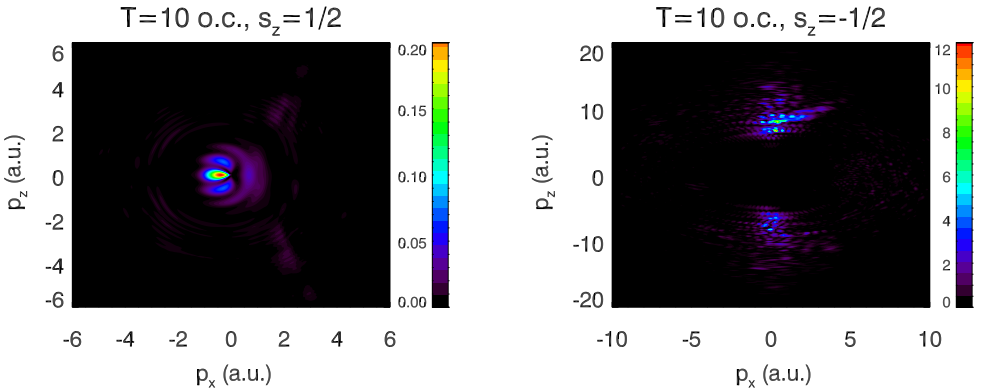

FIG. 7. Ionization probability distribution in the (p_x, p_z) plane for the pulse duration of $T = 10$ o.c. and field strength $F = 100$ a.u. Linear scale is used. Probability distribution for $s_z = -1/2$ is multiplied by a factor of 10^4.

pulse of $T = 5$ o.c. for an electric field strength as large as $F = 50$ a.u., and disappears completely for $F = 100$ a.u. It is, of course, quite natural that breakdown of the perturbation theory is delayed for a shorter pulse.

Momenta distributions for the field strength $F = 100$ a.u. in Fig. 6 look rather chaotic. One should bear in mind, however, that this impression is, to some extent, a consequence of the fact that a logarithmic scale has been used in this figure to reveal the fine details of the distributions. If we use a linear scale, the distributions look much more regular; an example is shown in Fig. 7, where we present distributions with and without spin flip for field strength $F = 100$ a.u. and pulse duration $T = 10$ o.c. Distribution for the spin-flip case still shows some rugged structures. A possible origin of these structures is discussed below.

Nondipole effects can be illustrated in a more compact form by presenting the probability distributions $W(\mu, p_x)$ for the electron momentum component p_x along the laser beam propagation direction (the so-called transverse electron momentum distribution or TEMD), which we computed as prescribed by Eq. (10). We present results for the electron spin projection $\mu = 1/2$ (ionization without a spin flip) and $\mu = -1/2$ (spin-flip ionization). In the nonrelativistic case, of course, the TEMD in the former case would be perfectly symmetric even functions of p_x, while TEMD in the latter would be identically zero. Distributions $W(\mu, p_x)$ with $\mu = \pm 1/2$ provide, therefore, a convenient characteristic of the ionization process, allowing one to gauge the role of the nondipole and spin effects.

Distributions $W(\mu, p_x)$ are shown in Figs. 8 and 9. Consider first the case of the $W(\mu, p_x)$ with $\mu = 1/2$, which has the nonrelativistic counterpart. The typical TEMD in the nonrelativistic case is an even function of the transverse momentum, possessing a cusplike singularity at zero transverse momentum [23]. The origin of this singularity is well studied. It is attributed to the strong Coulomb focusing effects [24], which lead to a formation of singularities (cusps) in the photoelectron spectra [20,23–25]. In the nonrelativistic case the strong field approximation (SFA) approach, neglecting the Coulomb potential altogether, does not reproduce this structure; one must use a modification, taking into account Coulomb effects, such as the Coulomb-Volkov distorted-wave approximation (CVA) [26].

It is known [6] that for the tunneling regime of ionization, already for the moderate field strengths (well below field strengths of the order of 1 a.u.) the nondipole effects, though not very pronounced yet, modify the TEMD. In [6] the authors performed a TDSE calculation taking full account of the nondipole effects for a model two-dimensional (2D) hydrogen atom and found that the TEMD, though still exhibiting the cusplike structures at small transverse momenta, becomes asymmetric. In our case, evolution of the TEMD without a spin flip follows the same pattern. With the increasing electric field the TEMDs, still preserving the cusplike singularity, develop asymmetric features, with a larger number of electrons escaping in the direction of the pulse propagation.

Distributions for the spin-flip ionization also exhibit cusp-like singularities, which probably have the same origin as in the case of the ionization without a spin flip. They are signatures of the effects introduced by the Coulomb field. The double-hump structure of the spin-flip TEMD observed in Figs. 8 and 9 for field strengths up to $F = 30$ a.u. can be explained by invoking the simple perturbative arguments we presented above. Spin-flip TEMD based on the perturbative ionization amplitude (17) would be an even function of p_x, having a dip at $p_x = 0$. This double-hump structure disappears with growing field strength and pulse length. As one can see from Figs. 8 and 9, for a field strength of $F = 50$ a.u. the perturbative picture provides a rather poor approximation for the shorter pulse of $T = 5$ o.c. and breaks down completely for the longer pulse of $T = 10$ o.c. Finally, for the highest field strength of $F = 100$ a.u. which we consider, the perturbation theory structures are obliterated completely. For this field strength, spin-flip distributions in Figs. 8 and 9 show complicated structures with several local maxima. These structures reflect the rugged structure of the spin-flip distributions in the (p_x, p_z) plane shown in Fig. 7. A question arises, of course: Are these structures real, or may they be just a consequence of the possible numerical inaccuracies of the calculation? As one can see from Figs. 8 and 9 the typical spin-flip ionization probability is six orders of magnitude smaller than the ionization probability without spin reversal (we provide below a simple explanation of this fact). Calculating such a small probability is generally a difficult task and we must ascertain that the required accuracy level has indeed been achieved. The accuracy checks we presented in Figs. 2 and 3 are of little help in solving this problem since

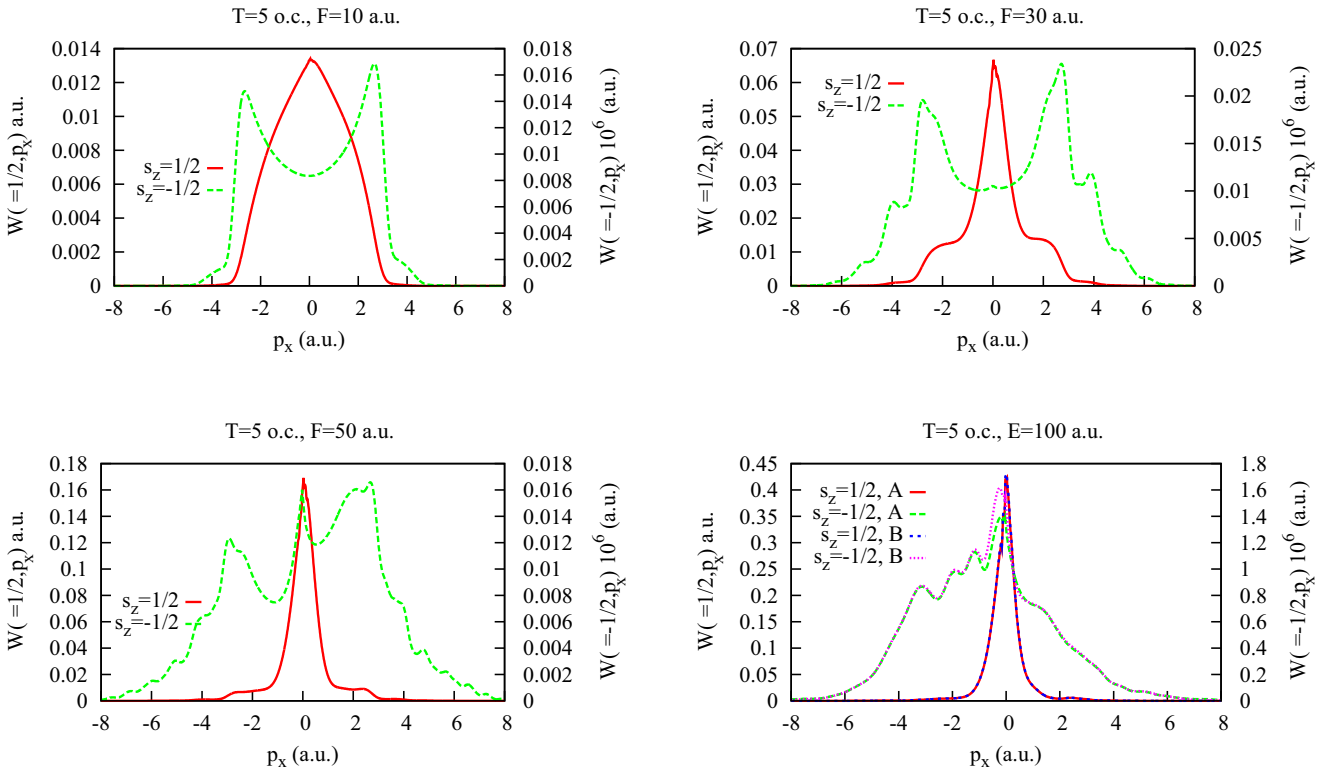

FIG. 8. Ionization probability distribution as a function of the momentum component in the pulse propagation direction for different field strengths, spin momentum projections, and pulse duration of 5 o.c. Results of two calculations (labeled A and B) are presented for $F = 100$ a.u. Calculation A used parameters $\Delta t = 0.0005$ a.u. and $J_{\max} = 65\frac{1}{2}$; calculation B used $\Delta t = 0.0003$ a.u. and $J_{\max} = 75\frac{1}{2}$.

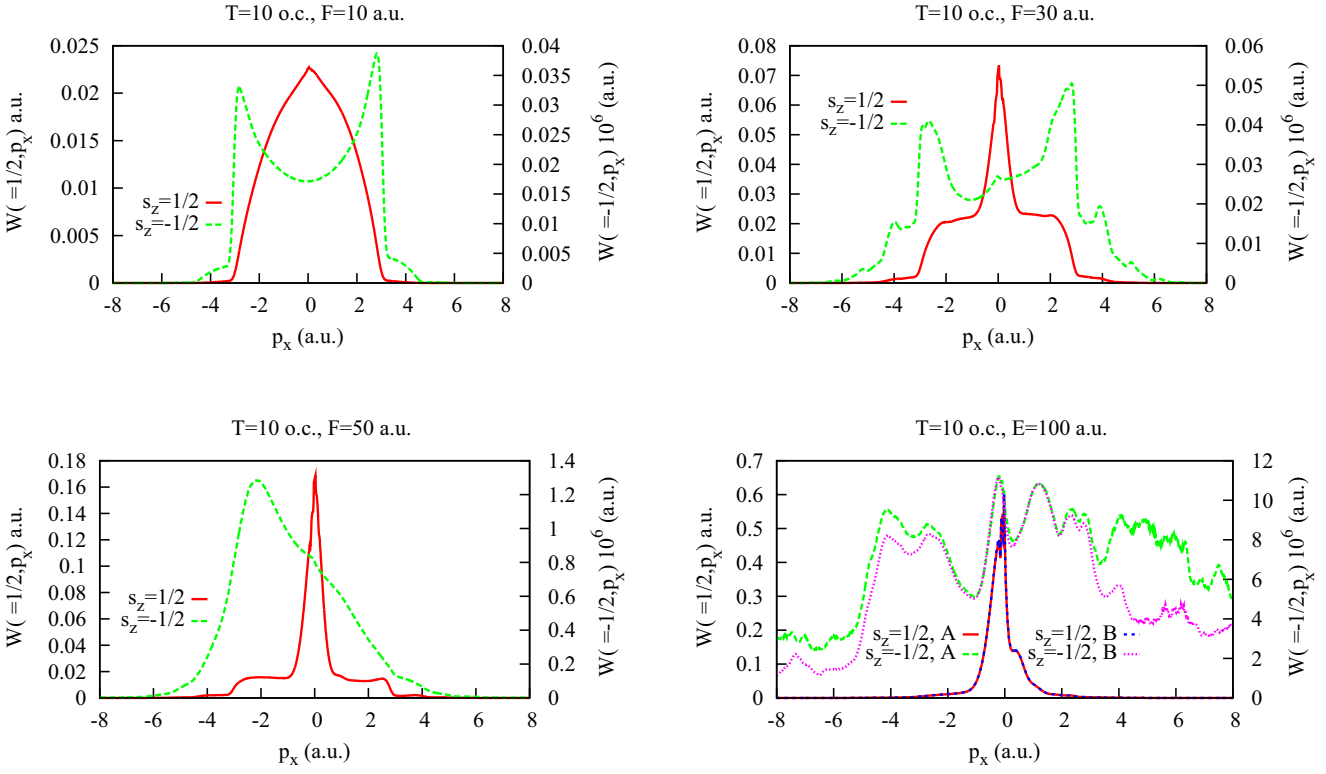

FIG. 9. Ionization probability distribution as a function of the momentum component in the pulse propagation direction for different field strengths, spin momentum projections, and pulse duration of 10 o.c. Results of two calculations (labeled A and B) are presented for $F = 100$ a.u. Calculation A used parameters $\Delta t = 0.0005$ a.u. and $J_{\max} = 65\frac{1}{2}$; calculation B used $\Delta t = 0.0003$ a.u. and $J_{\max} = 75\frac{1}{2}$.

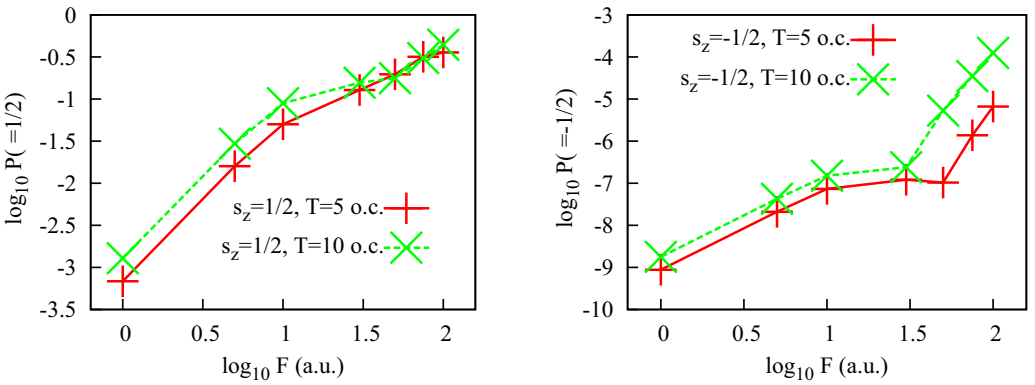

FIG. 10. Total ionization probability (logarithmic scale) as a function of $\log_{10} F$, where F is the pulse field strength in atomic units.

they present convergence tests for the ionization probability summed over the electron spin projections, which is by far dominated by the ionization without spin flip. We performed, therefore, additional accuracy checks for the field strength of $F = 100$ a.u. and total pulse durations of 5 and 10 o.c., and studied variations of the TEMD against variations of the essential parameters which may affect the overall accuracy: maximal total angular momentum $J_{\max}$ in the partial wave expansion (7), and time step Δt of the integration procedure. The additional calculation we performed for $F = 100$ a.u. and pulse durations of 5 and 10 o.c. (we refer to this calculation below as calculation B) used $\Delta t = 0.0003$ a.u. and $J_{\max} = 75\frac{1}{2}$. Calculation A used the parameters we indicated above: $\Delta t = 0.0005$ a.u. and $J_{\max} = 65\frac{1}{2}$, respectively. One can see that, for the ionization without spin flip, the curves showing the results of calculations A and B virtually coincide. Results for the spin-flip ionization for $F = 100$ a.u. show some differences between the two calculations. The origin of these differences is clear: even for the high field strengths we consider, the spin-flip ionization is a rather weak process, and its accurate numerical calculation poses serious difficulties. We may note, however, that the difference between calculations A and B for a pulse duration of 5 o.c. is very small, and is confined to a relatively small interval of the transverse momenta. For a pulse duration of 10 o.c., calculation B differs from A more significantly, especially for larger lateral momenta $p_x \gtrsim 4$ a.u. Even in this case, however, the central parts of the TEMD ($|p_x| \lesssim 4$ a.u.) agree well for both calculations, reproducing, in particular, the complicated structures with several local maxima. We can state with some certainty, therefore, that these structures are a real feature of the distributions.

The breakdown of the perturbation theory can be illustrated most conveniently by taking a look at the dependence of the total ionization probability upon the field strength. Figure 10 shows these dependencies for the ionization processes with and without spin flips. In addition to the results for $F = 10$, 30, 50, and 100 a.u. we discussed above, we added the results of additional calculations we performed for $F = 1$, 5, 10, and 75 a.u. to provide a more detailed picture. One can see that for the field strength $F \lesssim 10$ a.u. we are clearly in the perturbative regime, with $\log_{10} P(\mu) \approx a + N \log_{10} F$. As one can surmise from the data in Fig. 10, $N \approx 2$ for both $\mu = 1/2$ and $\mu = -1/2$. This corresponds, of course, to a one-photon ionization process driven by either $\hat{V}_z$ (ionization without spin flip) or $\hat{V}_x$ (spin-flip ionization) operators in Eq. (13). The ratio of the ionization probabilities with and without spin flip in the perturbative domain is, as one can see from Fig. 10, approximately 1×10^6. This can be understood easily from a simple estimate based on expressions (13) for the operators $\hat{V}_x$ and $\hat{V}_z$. Using these formulas, one can write for the ratio of the matrix elements $R = \langle f|\hat{V}_x|i\rangle/\langle f|\hat{V}_z|i\rangle$ (here $|i\rangle$, $|f\rangle$ are the initial and final atomic states) an estimate: $R \approx \omega^2 x/p_z/c^2$ [here we boldly substituted for x and p_z in Eqs. (13) typical atomic coordinate and momentum, and used estimates $A \approx F/\omega$ and $\frac{\partial H(t)}{\partial t} \approx \omega F$ for the vector potential and time derivative of the magnetic field in Eqs. (13)]. Using $x \approx 1$ and $p_z \approx 1$ for the ground state of atomic hydrogen, we obtain $R \approx 1.3 \times 10^{-3}$, which results in the ratio of the total ionization probabilities with and without spin flip: $P(\mu = -1/2)/P(\mu = 1/2) \approx R^2 \approx 1 \times 10^{-6}$.

For the field strengths exceeding $F = 10$ a.u. we are leaving the domain of the validity of the perturbation theory. Even for $F = 100$ a.u. the atom is not completely ionized, though. This is because of the high frequency of the driving pulse. A useful picture to judge the effect of the electromagnetic field on the atom is provided by the Kramers-Henneberger (KH) gauge [27,28]. Hamiltonian operators in the KH gauge and the velocity gauge are related by a canonical transformation [27], which leads to the KH Hamiltonian (we consider a completely nonrelativistic case here),

$$\hat{H}_{\rm KH} = \frac{\hat{\boldsymbol{p}}^2}{2} + V(\boldsymbol{r} + \boldsymbol{x}(t)), \tag{19}$$

where $\boldsymbol{x}(t) = \int_0^t \boldsymbol{A}\, d\tau$, $\boldsymbol{A}(t)$ is the vector potential of the pulse, and $V(\boldsymbol{r})$ is the potential energy in the atomic field-free Hamiltonian. $\boldsymbol{x}(t)$ is thus the classical displacement for the trajectory launched with initial zero coordinates and velocity in the field of the laser pulse. Its order of magnitude is $x \approx F/\omega^2 \approx 4$ a.u. for the the field strength $F = 100$ a.u. and frequency $\omega \approx 5$ a.u. we are using. For the displacement of this magnitude, $V(\boldsymbol{r} + \boldsymbol{x}(t))$ certainly differs considerably from the field-free atomic Coulomb potential $V(\boldsymbol{r})$, but some vestiges of the potential barrier still remain, thereby preventing total ionization of the atom.

IV. CONCLUSION

We considered ionization of a hydrogen atom in the field of ultrastrong laser pulses. We used a time-dependent Dirac equation as a calculational framework. Comparison of our results with the results of the calculations using the $\mathcal{P}$-space method [15], relying on the nonperturbative treatment of the nondipole effects, but neglecting the spin effects show good agreement of the results as long as we consider the region of relatively low energies not exceeding approximately $20\omega \approx 100$ a.u. The calculational framework relying on the solution of the TDDE allows one to include all relativistic effects, such as the nondipole, spin, and kinematic effects, barring, of course, the quantum electrodynamic (QED) effects, which are clearly outside the scope of the single-electron Dirac equation we consider. The latter effects, however, are completely negligible for the relatively low energies we consider.

Presented electron momenta distributions for the ionization process without the spin flip, which has a nonrelativistic counterpart, show a gradual increase of the role of nondipole effects, which manifests itself in destroying the $p_x \to -p_x$ symmetry which the nonrelativistic dipole momentum electron distributions possess. Use of the Dirac equation, which naturally incorporates the coupling of the spin and spatial variables, allowed us to consider ionization accompanied by a spin-flip process as well. Electron spectra in this case exhibit cusps, and some features (such as presence of a dip) are absent in the case of the ionization without the spin flip. These features can be explained, at least qualitatively, using the perturbation theory approach. Experimentally, the spin-flip ionization probability can be measured using a set of ideas suggested in [29], either preparing an initially polarized target of ions and detecting the photoelectron polarization in polarimetric experiments, or relating changes of the angular momentum of the ion and the electron's spin in the ionization process. In the latter case the spin-flip process will manifest itself in the difference of the ion angular distributions for circularly polarized laser fields with opposite helicities.

Alternative to the present method relying on the nonperturbative treatment of the relativistic effects might be a perturbative approach analogous to the one we followed in [7], where we included in the Hamiltonian effects of the first order in $\lambda = 1/c$, which is enough to describe the leading-order nondipole effects. The leading-order spin-flip effects, as we noted above, are of the order of λ^2. We might introduce a corresponding term to the Hamiltonian, adding for consistency other relativistic corrections of the order of λ^2, such as the leading-order kinematic correction, spin-orbit interaction, etc. That would lead essentially to the well-known Breit-Pauli Hamiltonian [22], containing additional terms describing the nondipole effects. We might then solve the TDSE using this Hamiltonian. There is, however, one important advantage in using the full Dirac Hamiltonian instead of the perturbative Breit-Pauli one. The Breit-Pauli spin-orbit interaction operator, for example, behaves as r^{-3} for small values of the radial coordinate [22]. Such an operator is, strictly speaking, not even self-adjoint, unless we narrow its domain of definition so that it acts only on the functions vanishing at the origin (otherwise its matrix elements may simply diverge due to the singular behavior of the integrand at the point $r = 0$). In the perturbative calculations this does not pose a problem, since selection rules due to angular integrations automatically ensure that with the proper choice of the basis of the nonrelativistic wave functions all radial integrals converge. In the nonperturbative calculation, such as solution of the TDSE with such an operator present in the Hamiltonian, this may lead to a problem of nonunitarity of the propagation operator. The way to cope with this problem might be to introduce suitable regularization for the spin-orbit interaction operator, so that its singular behavior at $r = 0$ is less severe. That would introduce, however, an additional parameter into the calculation, which would require careful checking that results are not very sensitive to its choice. Use of the Dirac Hamiltonian allows one to avoid this potential ambiguity altogether.

ACKNOWLEDGMENT

This work was supported by the Institute for Basic Science under Grant No. IBS-R012-D1.

[1] H. R. Reiss, J. Opt. Soc. Am. B **7**, 574 (1990).
[2] A. Ludwig, J. Maurer, B. W. Mayer, C. R. Phillips, L. Gallmann, and U. Keller, Phys. Rev. Lett. **113**, 243001 (2014).
[3] F. Krausz and M. Ivanov, Rev. Mod. Phys. **81**, 163 (2009).
[4] C. T. L. Smeenk, L. Arissian, B. Zhou, A. Mysyrowicz, D. M. Villeneuve, A. Staudte, and P. B. Corkum, Phys. Rev. Lett. **106**, 193002 (2011).
[5] S. Chelkowski, A. D. Bandrauk, and P. B. Corkum, Phys. Rev. Lett. **113**, 263005 (2014).
[6] S. Chelkowski, A. D. Bandrauk, and P. B. Corkum, Phys. Rev. A **92**, 051401(R) (2015).
[7] I. A. Ivanov, J. Dubau, and K. T. Kim, Phys. Rev. A **94**, 033405 (2016).
[8] V. S. Popov, B. M. Karnakov, V. D. Mur, and S. G. Pozdnyakov, Sov. Phys. JETP **102**, 760 (2006).
[9] M. Klaiber and K. Z. Hatsagortsyan, Phys. Rev. A **90**, 063416 (2014).
[10] E. Yakaboylu, M. Klaiber, and K. Z. Hatsagortsyan, Phys. Rev. A **91**, 063407 (2015).
[11] D. B. Milošević, Phys. Rev. A **93**, 051402 (2016).
[12] J. Feldhaus, J. Arthur, and J. B. Hastings, J. Phys. B **38**, S799 (2005).
[13] C. Gutt, L.-M. Stadler, S. Streit-Nierobisch, A. P. Mancuso, A. Schropp, B. Pfau, C. M. Günther, R. Könnecke, J. Gulden, B. Reime *et al.*, Phys. Rev. B **79**, 212406 (2009).
[14] L. Fang, M. Hoener, O. Gessner, F. Tarantelli, S. T. Pratt, O. Kornilov, C. Buth, M. Gühr, E. P. Kanter, C. Bostedt *et al.*, Phys. Rev. Lett. **105**, 083005 (2010).
[15] Z. Zhou and Shih-I Chu, Phys. Rev. A **87**, 023407 (2013).
[16] I. A. Ivanov, Phys. Rev. A **91**, 043410 (2015).
[17] A. Akhiezer and V. Berestetskii, *Quantum Electrodynamics* (John Wiley & Sons, New York, 1965).
[18] E. M. Lifshitz and V. B. Berestetskii, *Quantum Electrodynamics* (Pergamon Press, New York, 1982).

[19] M. Nurhuda and F. H. M. Faisal, Phys. Rev. A **60**, 3125 (1999).
[20] I. A. Ivanov, Phys. Rev. A **90**, 013418 (2014).
[21] I. A. Ivanov and A. S. Kheifets, Phys. Rev. A **89**, 021402 (2014).
[22] I. I. Sobelman, *Introduction to the Theory of Atomic Spectra* (Pergamon Press, New York, 1972).
[23] A. Rudenko, K. Zrost, T. Ergler, A. B. Voitkiv, B. Najjari, V. L. B. de Jesus, B. Feuerstein, C. D. Schröter, R. Moshammer, and J. Ullrich, J. Phys. B **38**, L191 (2005).
[24] A. S. Landsman, C. Hofmann, A. N. Pfeiffer, C. Cirelli, and U. Keller, Phys. Rev. Lett. **111**, 263001 (2013).
[25] A. N. Pfeiffer, C. Cirelli, A. S. Landsman, M. Smolarski, D. Dimitrovski, L. B. Madsen, and U. Keller, Phys. Rev. Lett. **109**, 083002 (2012).
[26] D. G. Arbó, J. E. Miraglia, M. S. Gravielle, K. Schiessl, E. Persson, and J. Burgdörfer, Phys. Rev. A **77**, 013401 (2008).
[27] H. A. Kramers, *Collected Scientific Papers* (North Holland, Amsterdam, 1956).
[28] F. Morales, M. Richter, S. Patchkovskii, and O. Smirnova, Proc. Natl. Acad. Sci. USA **108**, 16906 (2011).
[29] M. Klaiber, E. Yakaboylu, C. Müller, H. Bauke, G. G. Paulus, and K. Z. Hatsagortsyan, J. Phys. B **47**, 065603 (2014).